Ultrafast Optical Switching using PT-Symmetric Bragg Gratings

Sendy Phang,[1,*] Ana Vukovic,[1] Hadi Susanto,[2] Trevor M. Benson,[1] and Phillip Sewell,[1]

[1]*The George Green Institute for Electromagnetics Research, Faculty of Engineering, University of Nottingham, Nottingham, NG7 2RD, United Kingdom*
[2]*School of Mathematical Sciences, University of Nottingham, Nottingham, NG7 2RD, United Kingdom*
**Corresponding author: eexsp14@nottingham.ac.uk*

Received Month X, XXXX; revised Month X, XXXX; accepted Month X, XXXX; posted Month X, XXXX (Doc. ID XXXXX); published Month X, XXXX

This paper reports on time-domain modeling of an optical switch based on the PT-Symmetric Bragg grating. The switching response is triggered by suddenly switching on the gain in the Bragg grating to create a PT-Symmetric Bragg grating. Transient and dynamic behavior of the PT Bragg gratings is analyzed using the time-domain numerical Transmission Line Modeling (TLM) method including a simple gain saturation model. The on/off ratio and the switching time of the PT-Bragg grating optical switch are analyzed in terms of the level of gain introduced in the system and the operating frequency. The paper also discusses the effect the gain saturation has on the operation of the PT-Symmetric Bragg gratings.

OCIS codes: 230.0230, 190.0190.

1. INTRODUCTION

Recently a new class of optical waveguides, that compensates the inherent loss of photonic material by introducing gain, has opened new ways for the realization of functionalities such as unidirectional invisibility [1,2], double refraction and power oscillation [3], lasing and absorber cavities [4,5], isolating and beam-steering behavior [6] and optical switching [7,8,9]. By carefully combining gain and loss in an optical waveguide, the system mimics the complex Parity-Time (PT) symmetric potential in quantum physics [10], with the main characteristic that below a certain gain/loss level the system operates in the stable regime and above this point the system exhibits energy growth [11]. Several different PT-symmetric structures have been investigated including PT-symmetric Bragg gratings [1,12], grating-assisted couplers [13,14] , coupled waveguides [6,15,16] and lattices [2,3,11]. Experimentally, PT waveguide couplers have been demonstrated on a $LiNbO_3$ platform where one waveguide was providing gain and the other an equal amount of loss [17].

In this paper we focus on the application of optical switching using PT-symmetric Bragg gratings. Ultra-fast optical switches typically exploit the strong third order nonlinearity, or Kerr nonlinearity, of photonic materials. Optical switches of this type have been reported using nonlinear Bragg gratings [18], silicon waveguides [19] and photonic lattices [20], with the switching time varying from 2ns [19] to 50ps [20]. Although several papers mention the possibility of realizing optical switches using PT-symmetric structures, the actual operation of a PT-grating in the time domain has not been numerically demonstrated. This is mainly due to the fact that the modeling of PT-symmetric structures has been done exclusively in the frequency domain using Coupled Mode Theory (CMT) [12,15], the transfer matrix method [1,21,22], Floquet-Bloch theory [3] and modal analysis [23]. Although frequency domain analysis can provide valuable insight into the behavior of the PT-structures, it is incomplete if transient and real-time responses are also of interest.

The purpose of this paper is to investigate and report on the application of the PT Bragg grating as an optical switch, where the switching response is triggered by suddenly switching on the gain in the system. A simple frequency independent gain saturation model [24] is also used in this work. The Kramers-Kronig relations between the real and imaginary part of the refractive index are not taken into account. The Kerr nonlinearity is not considered in this paper, although it is expected that it may further enhance switching operation [1].

Throughout this work the established Transmission Line Modeling (TLM) numerical method is used [25,26]. This is a flexible time stepping numerical technique that has been extensively characterized and used over many years [25,26,27]. However, any time domain method, including the Finite-Difference Time Domain Method (FDTD), could be employed for this purpose and we refer to the extensive literature for further details of both of these algorithms. It is appropriate to comment that the TLM method has comparable performance with the FDTD method but offers certain advantages for particular applications [28,29].

The paper is organized as follows: in the next section a description of the PT-Bragg structure considered in this paper is given, together with a brief outline of the TLM method. Section 3 validates the accuracy of the TLM method with a gain saturation model when applied to the PT Bragg structure by comparing its results with the analytical method based on the transfer matrix (T-matrix) method [30], and investigates the dispersion properties of the PT Bragg grating for different values of gain and loss in the grating. The gain saturation model and its effects on the response of the PT-Bragg grating for low and high input field intensities is also discussed. Section 4 demonstrates the switching operation of the PT Bragg grating when the gain is switched in real time in the grating. A practical scenario is

considered whereby the grating is considered to be a lossy Bragg grating and once steady-state is achieved, the gain is switched locally on gain sections to create a PT-Symmetric Bragg grating. Furthermore the design parameters for the PT-Bragg grating switch are analyzed for optimal switching time and on/off ratio. Section 5 outlines the main conclusions of the paper.

2. THE PT-SYMMETRIC BRAGG GRATING STRUCTURE AND THE TLM MODEL

PT-symmetry structures in photonics, are structures with balanced gain and loss, require that a complex refractive index profile satisfies the condition $\hat{n}(x) = \hat{n}^*(-x)$, which means that the real part of the refractive index is an even function of the position x, and the imaginary part of the refractive index, which represents gain or loss, is an odd function of position [4,17]. In this paper a PT Bragg grating with piecewise constant layers of refractive index $\hat{n} = (n_R \pm \Delta n_R) \pm j n_I$ is considered, where n_R is the average refractive index of the grating, and Δn_R and n_I are the modulations of the real and imaginary part of refractive index, respectively. The grating is surrounded by refractive index n_R and has length $N\Lambda$ where Λ is the length of one period as shown in Fig. 1(a). Fig. 1(b) shows the refractive index profile for one period of the grating, with solid and dashed lines representing the real and imaginary refractive index profile respectively. Fig. 1(b) shows that each period, Λ, consists of four different layers of the same thickness so that $\Lambda = \lambda_B/(2n_R)$, where λ_B is the Bragg wavelength.

In the absence of loss and gain i.e. $n_I = 0$, the structure reduces to a conventional Bragg grating that exhibits the highest reflection at the Bragg frequency and the device has a reciprocal response, i.e. the transmission and the reflection are the same regardless of whether the excitation is coming from the left- or the right-hand side of the grating. The addition of gain and loss in the system modifies its properties and although the transmission remains the same for the left and right excitation, the reflection is different due to the different input impedances observed from each end of the grating. Here we would like to emphasize that although a PT-symmetric Bragg grating has often been regarded as a nonreciprocal structure [3,17], in a strict sense the PT-symmetric Bragg grating satisfies the Lorentz reciprocity condition as long as it is linear [23,31] because the scattering matrix $\bar{\bar{S}}$ is always a complex symmetric matrix ($\bar{\bar{S}} = (\bar{\bar{S}})^T$) [4] although it is no longer unitary/orthogonal ($(\bar{\bar{S}})^{-1} \neq (\bar{\bar{S}})^\dagger$), where T and † are the transpose and transpose-conjugate operators respectively. Two particular modes of operation that have attracted interest are the Unidirectional (U) operation [1,2] and Coherent Perfect Absorber-Laser (CPAL) operation [4,5]. Unidirectional operation occurs when the real index modulation equals the gain/loss parameter, i.e. $\Delta n_R = n_I$. In this mode the Bragg grating exhibits unidirectional invisibility when excited from the right side, i.e. there is negligible reflection and all power is transmitted through the grating [1]. The CPAL operation occurs for a particular value of n_I ($n_I > \Delta n_R$) for which one pole and one zero of the scattering matrix $\bar{\bar{S}}$ overlap on the imaginary axis in the complex frequency plane [4] and thus the grating acts as an absorber and laser at the same time. It is important to note that at the CPAL point, the absorption occurs with lasing simultaneously [5] and is independent of the incident signal location (left or right). Further increase of gain/loss in the grating causes more zeroes and poles to cross over the imaginary axis, thus inducing instability and the grating exhibits exponential energy growth.

Here the TLM method is used to investigate the time-domain response of the PT Bragg grating structure. The TLM method is based upon the analogy between the propagating electromagnetic fields and voltage impulses traveling on an interconnected mesh of transmission lines. Successive repetitions of a scatter-propagate procedure provide an explicit and stable time stepping algorithm that mimics electromagnetic field behavior to second order accuracy in both time and space [25,26]. In its simplest, one-dimensional (1D), form the TLM method discretizes the problem of interest into sections of length Δx, represented by a transmission line model. The accuracy of the method is dependent on adequate discretization of the model, and typically, for an uniform medium, it is required that $\Delta x < \lambda/10$, where λ is the lowest wavelength of interest. A segment Δx of the 1D TLM node is shown in Fig. 2, and described in detail in [26], where L_0 and C_0 denote the magnetic and dielectric properties of the free space. Material dielectric properties and the gain/loss are represented by additional capacitance ΔC and conductance G respectively. The real part of the refractive index is modeled by ΔC as

$$\Delta C = \epsilon_0 \, Re\left(\hat{n}^2 - 1\right) \Delta x, \tag{1}$$

whilst the conductivity G models the gain/loss n_I as

$$G = -2 \, \omega_B \, Re(\hat{n}) \, Im(\hat{n}) \, \Delta x, \tag{2}$$

where ω_B is the Bragg angular frequency. In this paper saturation of the gain is implemented in the general form [24],

$$G = \frac{G_0}{1 + (E/E_{sat})^{2k}} \tag{3}$$

where G_0 is the initial gain/loss parameter value in absence of electric field, E and E_{sat} denote the electric field in the material and at the saturated state respectively and k is the order of saturation. The model saturates gain at high field intensities in order to avoid unbounded energy growth within the structure while providing an unsaturated (linear) and frequency independent gain at low field intensity. The exact parameters for the saturated field E_{sat} and the order of saturation, k, are material dependent and obtained by measurement.

The equivalent circuit of the spatial TLM segment Δx shown in Fig. 2 indicates strong physical intuition between the lumped circuit and physical phenomena which is an appealing feature of the TLM method compared to other purely numerical techniques. Implementation of material properties, such as gain and loss, in the TLM method is straightforward and as such the method is ideally suited to model non-linear and time-varying material behavior. The TLM method has been used to model linear, nonlinear and dispersive one-dimensional (1D) Bragg gratings [32]. For further details of how this is implemented in the TLM method and applied to a 1D Bragg grating the reader is referred to [32,33,34].

3. TIME-DOMAIN MODELING OF PULSE PROPAGATION THROUGH THE PT-BRAGG GRATING

In this section the results obtained using the TLM model for the PT-Bragg grating are compared with the analytical ones obtained using the transfer matrix (T-matrix) method [30]. The methodology of the T-matrix method is not presented in this

paper and the reader is referred to [30]. The T-matrix method models a linear structure, i.e. it does not include the gain saturation behavior. The TLM results are obtained for two different regimes, i.e. when the grating is excited with a low and high intensity signal with respect to the gain saturation electric field E_{sat}.

The PT Bragg grating considered in this paper consists of 150 periods, with an average index $n_R = 1.55$, real index modulation $\Delta n_R = 0.01$ and operated at/around a Bragg wavelength $\lambda_B = 1\mu m$. The grating is surrounded by a medium of refractive index n_R. The refractive index of 1.55 was that used in [12]. The authors of [12] do not specify the material, but this refractive index would be typically of silicon-oxynitride (SiON) where a value of $\Delta n_R = 0.01$ could be achieved by changing the oxygen-nitrogen ratio [35]. Our initial investigation of the effect of the sampling on the accuracy of the TLM model confirmed that results are highly sensitive to the spatial sampling with a sampling size of $\Delta x = \lambda/96$ necessary for good agreement with the T-matrix results, where λ is the Bragg wavelength in the medium of n_R [36].This is in agreement with results obtained previously for modeling linear Bragg gratings, where sampling size was required to be $\Delta x < \lambda/48$, [32], taking into account that the structural element of a PT grating is half of that of the linear Bragg grating. For this reason we use a sampling size of $\Delta x = \lambda/96$ for the rest of the paper. The frequency response is obtained by Fourier transformation of the time-domain signal. The TLM simulation was run for $NT = 262144$ time-steps which ensured that all the signal has passed through the structure and provided a sufficient frequency domain resolution.

Fig. 3 investigates the impact of the gain and loss parameter n_I and input signal amplitudes on the operation of the PT Bragg grating using result obtained with the T-matrix [30] and the TLM methods. The input signal is a continuous wave (CW) at the Bragg frequency. The effect of the gain saturation is studied in a general manner by normalizing the input field amplitude E_m with the E_{sat} parameter. The order of saturation is initially taken to be $k = 4$. We consider TLM responses for two cases, namely when the grating is excited by: (a) a small signal amplitude $E_m = 0.002E_{sat}$ and (b) a high signal amplitude $E_m = 0.2E_{sat}$. Fig. 3 shows the normalized transmitted and reflected power for the left (Γ_L) the right (Γ_R) incidence. The T-matrix results for the transmitted power are presented by T (which is theoretically the same for the left and right incidence). The TLM results of normalized transmitted power are represented by T_L (for left incidence) and T_R (for right incidence). The reflectance of the PT-Bragg grating is represented by Γ_L for the left incidence and Γ_R for the right incidence, for both analytical and TLM results.

Fig. 3(a) compares TLM and analytical results in the low intensity regime ($E_m = 0.002E_{sat}$) and shows that TLM results agree very well with the T-matrix results before the CPAL point. However, when operating beyond the CPAL point both the transmission and reflection increase and the grating exhibits energy growth. It is here emphasized that beyond the CPAL point i.e. when the poles and zeros have crossed the imaginary axis, the grating system is working in an unstable regime [4] which is confirmed by the TLM method. Furthermore, the TLM results also imply that as the electric field intensity inside the structure increases, the effect of gain saturation dominates therefore gain and loss within the structure are no longer balanced and thus the structure is no longer PT-symmetric. It is depicted in the inset of the Fig. 3(a) that above the CPAL point the gain saturation modifies the TLM response of the transmittance which is no longer reciprocal ($T_L \neq T_R$).

Fig. 3(b) shows the transmitted and reflected powers for a higher input CW signal amplitude, i.e., $E_m = 0.2E_{sat}$. As shown in the figure, the gain saturation starts to take effect at a lower value of gain/loss parameter, $|n_I| > 0.01$, compared with the situation shown by Fig. 3(a), $|n_I| > 0.0129$. It implies that when the grating is initiated with stronger input signals the gain saturation starts to take effect at lower gain/loss parameter n_I below the theoretical CPAL point. Again the inset of Fig. 3(b) shows that when the gain saturates the response of the transmission is no longer reciprocal i.e. $T_L \neq T_R$. Both Fig. 3(a,b) demonstrate that when the gain saturates, the grating acts as a laser cavity regardless of the incident signal direction with an output power from the left (gain) side higher than the right (loss) side.

Fig. 3(a,b) further shows that as the gain/loss is increased from zero up to $n_I = 0.01$ in the grating, the transmitted power T increases whereas Γ_R decreases and Γ_L increases. For the gain/loss parameter $n_I = \Delta n_R = 0.01$, when the PT Bragg grating is excited from the right, there is negligible reflection ($\Gamma_R = 0$) and all power is transmitted ($T = 1$). Thus the grating acts as the background medium i.e. it is invisible when excited from the right, (U point in Fig.3). Alternatively, when excited from the left, all power is again transmitted ($T = 1$) but the reflection Γ_L is increased. This non-reciprocal response means that at the U point the grating is exhibiting unidirectional invisibility. In addition Figs. 3(a,b) show very good agreement between the TLM and T-matrix results at lower gain/loss parameters n_I at which Bragg grating operates in the linear regime, i.e. the gain saturation does not take effect.

Fig. 4 shows the impact of the input field intensity on the "gain saturation point" for different saturation order, k. The gain saturation point is here taken as the value of gain/loss parameter n_I for which the transmittance splits, i.e., $|T_L - T_R| > 10^{-3}$. The U and CPAL point are also marked on the graph for reference. Three different input amplitudes are considered, namely $E_m = 0.002E_{sat}$, $E_m = 0.1E_{sat}$ and $E_m = 0.2E_{sat}$. It can be seen that increasing the input field amplitude causes the gain saturation to take effect at lower values of gain/loss n_I in the grating thus effectively reducing the linear operating regime.

Fig. 5 shows the frequency response of the grating for different gain/loss parameters i.e. $n_I = 0, 0.005$ and 0.01 obtained by using the TLM method for different input signal amplitudes. The input for this calculation is a Gaussian pulse function at the Bragg frequency with a full width half-maximum (FWHM) of 0.015ps. Three cases of normalized input amplitudes are considered, namely $E_m = 0.2E_{sat}$, $E_m = 0.8E_{sat}$ and $E_m = E_{sat}$. The results are shown with respect to detuning factor $\delta = \omega - \omega_B$, where ω and ω_B are the angular frequency and the Bragg angular frequency respectively. The frequency response is obtained by Fourier transforming the time-domain signal response. Fig. 5 shows that for $n_I = 0$ the response corresponds to the conventional Bragg filter with a stopband centered at the Bragg frequency and $\Gamma_R = \Gamma_L$. As the gain/loss parameter is increased the band-gap decreases, the reflection from the left, Γ_L, is increased, whilst the reflection from the right Γ_R, is decreased. For $n_I = 0.01$ and $E_m = 0.2E_{sat}$ (the U point in Fig. 3(b)) the transmittance is almost one for all frequencies, Γ_L in the stopband is increased and Γ_R is negligible.

Furthermore, comparing the inset of Fig. 5(a and c), it can be seen that the transmittance for the left and right incident is no

longer equal, $T_L \neq T_R$ for $E_m = E_{sat}$, showing that the presence of gain saturation breaks the balance of gain and loss even below the U point.

Fig. 6 shows the temporal response of the PT Bragg grating where transmitted signals are shown for three different cases of gain/loss in the grating namely, (a) for $n_I = 0.0025$ (below the U point), (b) at the U point $n_I = 0.01$, and (c) above the CPAL point at $n_I = 0.013$. The input signal is a Gaussian pulse function at the Bragg frequency having an amplitude of $E_m = 0.2E_{sat}$ and FWHM $= 0.015$ps. Fig. 6(a) shows the transmitted signal normalized to the input signal for $n_I = 0.0025$, with the normalized input signal shown in the inset. It can be seen that when the grating is operating below the U point the signal experiences strong dispersion. Fig. 6(b) shows the output signal normalized to the input signal when the grating is operating at the U point demonstrating the preservation of the signal shape; the signal experiences negligible dispersion and no net gain/loss.

Fig. 6(c) shows the normalized transmitted signal at $n_I = 0.013$, operation above the CPAL point, for two different TLM models, i.e., with and without gain saturation model. As can be seen, without a built-in gain saturation model there is an exponential growth of field intensity as the device operates in the unstable regime. On the other hand, the response of the TLM with a gain saturation model included yields a saturated output signal. The output signals obtained with and without gain saturation propagate in phase, as can be seen in the inset of Fig.6(c). The results imply that in the steady-state at and above CPAL point, the PT-symmetric Bragg grating operates in a non-linear regime and behaves as a Fabry-Perot laser cavity with lasing frequency f_B.

In the following section we will demonstrate the switching operation of the PT-Bragg grating when it operates in the linear regime below and around U point with balanced loss and gain.

4. PT BRAGG GRATING AS OPTICAL SWITCH

This section investigates the transient and dynamic behavior of a PT-Bragg grating where the gain is suddenly introduced into parts of the system. Furthermore, the switching operation of the PT-Bragg grating is analyzed for different values of gain/loss and different operating frequencies. The PT-Bragg grating considered in this section is as described in Fig. 1 and studied in the previous section.

The scenario that is modeled is as follows: initially, the Bragg grating is assumed to be uniformly lossy ($n_I = -0.01$) throughout, under which conditions the grating has a principal stopband centered at the Bragg frequency. Once the grating is operating in the steady state the gain is introduced as might be achieved practically by laser beam pumping gain sections while masking the lossy sections [17]. We first consider a case where the grating is excited with a CW wave at the Bragg frequency with a signal amplitude $E_m = 0.2E_{sat}$. At $t = 3$ps, when the grating is in steady state, the gain is switched to $n_I = 0.01$. The choice of input signal amplitude ensures that the PT-symmetric Bragg grating operates in the linear regime, i.e. the effect of gain saturation is small, as discussed in Section 3.

Fig. 7 shows the time domain response and the frequency content for the input-normalized transmitted and reflected signals of the PT optical switch, for the left and right excitation. Figs. 7(a,b) and (c,d) show the input-normalized transmitted and reflected signal when the grating is excited from the left (T_L,Γ_L) and right (T_R,Γ_R), respectively. It can be seen that the transmittance T_L and T_R changes from nearly 0 to ≈ 1 over the transient period of about 0.4ps.

Figs. 7(b,d) show that the Γ_L has increased but Γ_R has sharply reduced to almost zero. The results confirm that if the grating is excited from the right, its response will change from purely reflective to all transmitting and thus exhibits a switch-like behavior. It is also emphasized that this is achieved when the grating is operated at the Bragg frequency with a background medium of n_R and to our knowledge this is the first demonstration of a temporal PT-Bragg grating switch using a numerical time-domain code.

Figs. 7(e,f,g,h) show the frequency content of the time-domain response with (solid line) and without (dashed line) the switching of the gain/loss parameter. It can be noticed that, apart from the obvious changes in the amplitudes, the transmitted and reflected signals have broader spectra due to the strong transients caused by switching.

Fig.7 demonstrates that switching of gain and loss in the grating in the real time triggers a switch-like response from the grating. The impact of the gain/loss parameter (n_I) and operating frequency on switch response, i.e., on/off ratio and switching time, is investigated in Fig. 8 and Fig. 9.

Fig. 8 investigates the impact of the operating frequency on the performance of the optical switch. The initial grating is assumed to be lossy ($n_I = -0.01$) and when the steady state is reached, for example, at $t = 3$ps, the gain is switched to $n_I = 0.01$ (U point). The grating is excited with a continuous wave (CW) signal at, and around, the Bragg frequency. Of particular interest is the case of the right incidence where an increase of transmission is accompanied by reduction in reflection. Fig. 8 shows how the change of detuning of the angular frequency from the Bragg frequency ($\delta = \omega - \omega_B$) affects the switching time and the on/off ratio of the transmitted signal. As expected, the maximum on/off transmittance ratio is achieved at the Bragg frequency. The on/off ratio depends more strongly on the operating frequency, whilst the switching time remains in the region of $0.4 - 0.8$ps for the range of frequencies studied.

Fig. 9 depicts the on/off ratio and the switching time of the PT Bragg optical switch for different values of gain/loss parameter, n_I. The operating frequency is set to be the Bragg frequency. Fig. 9 shows that on/off ratio increases as the gain/loss parameter is increased. For all values of gain/loss the switching time remains below 1.4ps with a minimum at $n_I = 0.01$ (U point). It is understood that the practical switching time will also include the time needed to create gain in the structure[37].

5. CONCLUSION

The paper reports on the time-domain modeling of PT-Bragg gratings using the numerical TLM time domain method with a gain saturation model. The effect of the gain saturation model on the PT-grating response is discussed under conditions of low and high input intensity excitation. The results show that the response of the grating at high input intensities effectively reduces the linear operating regime with respect to the gain/loss parameter n_I.

The paper further shows that an optical switch can be engineered by suddenly switching the gain in the grating and ensuring that the grating is operating in the linear regime. The on/off ratio in the transmitted amplitude is maximum and switching times are minimum when the grating is operating at

the U point. The time-domain simulation of the switching operation also shows that the presence of strong transients due to the sudden switching of the gain broadens the spectrum of the transmitted signal.

REFERENCES

1. Z. Lin, H. Ramezani, T. Eichelkraut, T. Kottos, H. Cao, and D. N. Christodoulides, "Unidirectional invisibility induced by PT-symmetric periodic structures," Phys. Rev. Lett., vol. 106, no. 213901 (2011).
2. A. Regensburger, C. Bersch, M. A. Miri, G. Onishchukov, D. N. Christodoulides and U. Peschel, "Parity-time synthetic photonic lattices," Nature, vol. 488, pp. 167-171, (2012).
3. K. G. Makris, R. El-Ganainy, and D. N. Christodoulides, "Beam dynamics in PT symmetric optical lattices," Phys. Rev. Lett., vol. 100, no. 103904 (2008).
4. Y. D. Chong, L. Ge, and A. D. Stone, "PT-symmetry breaking and laser-absorber modes in optical scattering systems," Phys. Rev. Lett., vol. 106, no. 093902 (2011).
5. J. Schindler, Z. Lin, J. M. Lee, H. Ramezani, F. M. Ellis, and T. Kottos, "PT-symmetric electronics," J. Phys. A: Math. Theor., vol. 45, no. 444029 (2012)
6. T. Kottos, "Broken symmetry makes light works," Nature Physics, vol. 6, pp. 166-167 (2010).
7. H. Ramezani, T. Kottos, R. El-Ganainy and D. N. Christodoulides, "Unidirectional nonlinear PT-symmetric Optical structures," Phys. Rev. A., vol. 82, no. 043803 (2010)
8. A. A. Sukhorukov, Z. Xu, and Y. S. Kivshar, "Nonlinear suppression of time reversals in PT-symmetric optical couplers," Phys. Rev. A, vol. 82, no. 043818 (2010).
9. F. Nazari, M. Nazari, and M. K. Moravvej-Farshi, "A 2×2 spatial optical switch based on PT-symmetry," Optics Letters, vol. 36, no. 22 (2011)
10. C. M. Bender, S. Boettcher, and P. N. Meisinger, "PT-symmetric quantum mechanics," Journal of Mathematical Physics, vol. 40, pp. 2201 - 2229 (1999).
11. S. Nixon, L. Ge, and J. Yang, "Stability analysis for soliton in PT-symmetric optical lattices," Phys. Rev. A., vol. 85, no. 023822 (2012).
12. M. Kulishov, J. M. Laniel, N. Belanger, J. Azana, and D. V. Plant, "Nonreciprocal waveguide Bragg gratings," Optics Express, vol. 13, no. 8 (2005).
13. M. Greenberg, and M. Orenstein, "Unidirectional complex grating assisted couplers," Opt. Express, vol. 12, no. 17 (2004)
14. M. Greenberg, and M. Orenstein, "Optical unidirectional devices by complex spatial single sideband perturbation," IEEE J. Quantum Electron, vol. 41, no. 7 (2005)
15. R. El-Ganainy, K. G. Makris, D. N. Christodoulides, and Z. H. Musslimani, "Theory of coupled optical PT-symmetric structures," Opt. Lett., vol. 32, pp. 2632-2634 (2007).
16. L. Chen, R. Li, N. Yang, and L. Li, "Optical modes in PT-symmetric double channel waveguides," in *Proceeding of The Romanian Academy, series A*, vol. x, no. x, pp. 1-10 (2012).
17. C. E. Rüter, K. G. Makris, R. El-Ganainy, D. N. Christodoulides, M. Segev, and D. Kip, "Observation of parity-time symmertry in optics," Nature Physics, vol. 6, 192-195 (2010).
18. A. Melloni, M. Chinello, M. Martinelli, "All-Optical switching in phase shifted fibre Bragg grating", IEEE Photon. Techn. Letters, Vol.12, No.1 (2000).
19. Y. Vlasov, W. M. J. Green, F. Xia, "High-throughput silicon nanophotonic wavelength-insensitive switch for on-chip optical networks", Nature Photonics, Vol. 2, 242-246 (2008).
20. A. Majumdar, M. Bajcsy. D. Englund, J. Vuckovic, "All optical switching with a single quantum dot strongly coupled to a photonic crystal cavity", IEEE J. Selected Topics in Quantum Electron., Vol.18, No.6 (2012).
21. A. Mostafazadeh, "Invisibility and PT-symmetry," *ArXiv e-prints*, vol. 1206, no. 0116 (2012).
22. A. Mostafazadeh, "Spectral singularities of complex scattering potentials and infinite reflection and transmission coefficients at real energies," Phys. Rev. Lett, vol. 102, no. 220402 (2009).
23. J. Čtyroký, V. Kuzmiak, and S. Eyderman, "Waveguide structures with antisymmetric gain/loss profile," Optics Express, vol. 18, no. 21 (2010).
24. A. E. Siegman, *Lasers* (University Science Books, 1986).
25. W. J. R. Hoefer, "The transmission-line matrix method - theory and applications," IEEE Transactions on Microwave Theory and Techniques, vol. 33, pp. 882-893, (1985).
26. C. Christopoulos, *The Transmission Line Modeling Method: TLM* (IEEE Press, 1995).
27. M. Krumpholz, C. Huber, P. Russer, "A field theoretical comparison of FDTD and TLM", IEEE Trans., MTT, Vol.43, No.8, pp.1935-1950, 1995.
28. M. N. O. Sadiku, "A comparison of time-domain finite difference (FDTD) and transmission-line modeling (TLM) methods," in *Proceeding of IEEE Southeastcon 2000* (IEEE, 2000), pp. 19-22.
29. P. B. Johns, "On the relationship between TLM and finite-difference methods for Maxwell's equation," IEEE Micro. Theo. Tech. vol. 35, no. 1, (1987).
30. R. E. Collin, *Field Theory of Guided Waves*, 2nd Edition, (IEEE Press, 1991).
31. D. Jalas, A. Petrov, M. Eich, W. Freude, S. Fan, Z. Yu, R. Baet, M. Popovic, A. Melloni, J. D. Joannopoulos, M. Vanwolleghem, C. R. Doerr, and H. Renner, "What is – and what is not an optical isolator," Nature Photonics, vol. 7, pp. 579-582 (2013)
32. V. Janyani, A. Vukovic, J. D. Paul, P. Sewell and T. M. Benson, "The development of TLM models for nonlinear optics," IEEE Microwave Review, vol. 10, no. 1 (2004).
33. J. Paul, C. Christopoulos, and D. W. P. Thomas, "Generalized material modes in TLM-part 3: material with nonlinear properties," IEEE Trans. Antennas Propagat., vol. 50, pp. 997-1004 (2002).
34. J. Paul, C. Christopoulos, and D. W. P. Thomas, "Generalized material model in TLM-part I: material with frequency-dependent properties," IEEE Trans. Antennas Propagat., vol. 47, no. 10 (1999).
35. K. Wörhoff, L. T. H. Hilderink, A. Driessen, and P. V. Lambeck, "Silicon oxynitride a versatile material for integrated optics applications," Journal of the electrochemical society, vol. 149, no.8, (2002)
36. S. Phang, A. Vukovic, H. Susanto, T. M. Benson, and P. Sewell, "Time Domain Modeling of All-Optical Switch based on PT-Symmetric Bragg Grating," in *Proceedings of The 29th Annual Review of Progress in Applied Computational Electromagnetics (ACES)*, March 20-28, 2013, Monterey, CA, (ACES, 2013), pp. 693-698.
37. C. Larsen, D. Noordegraaf, P. M. W. Skovgaard, K. P. Hansen, K. E. Mattsson, and O. Bang, "Gain-switched CW fibre laser for improved supercontinuum generation in a PCF," Optics Express, vol. 19, no. 16 (2011)

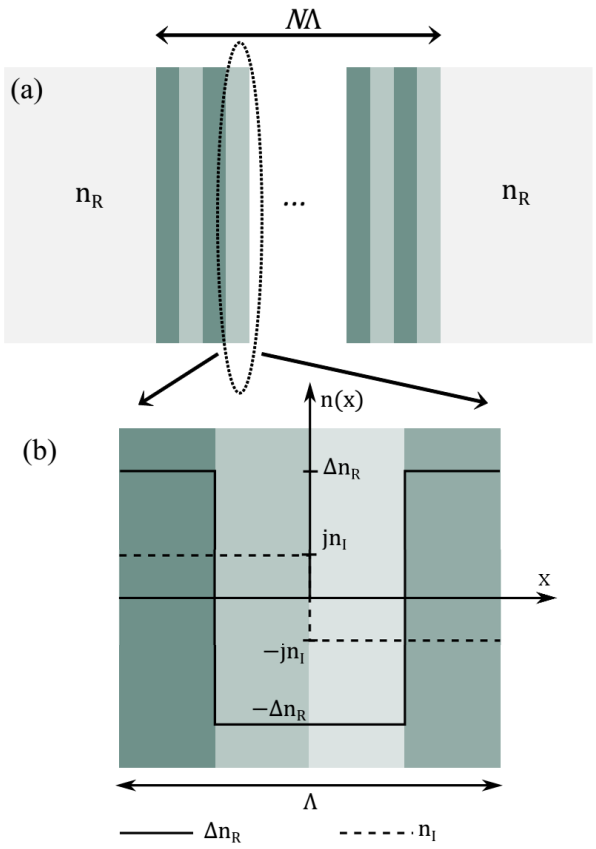

Fig. 1. (Color online) Schematic presentation of (a) the PT Bragg grating and (b) the refractive index profile for one period of the grating.

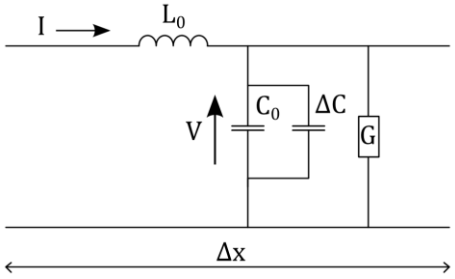

Fig. 2. A single segment of one dimensional TLM meshing.

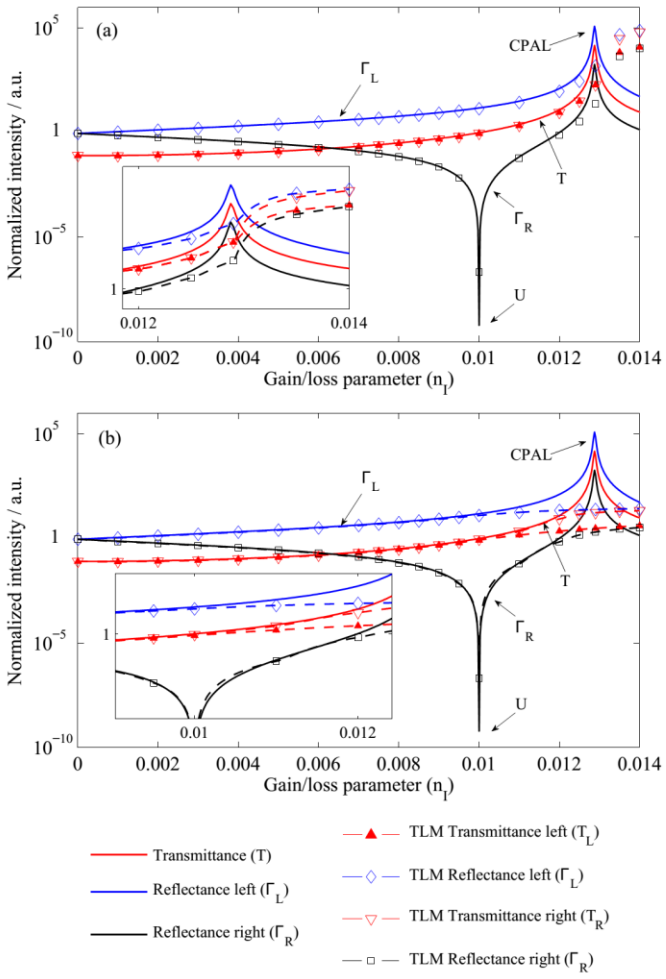

Fig 3. (Color online) Comparison of the TLM and T-matrix results for the transmitted power from left (T_L) and right (T_R), power reflected from the left (Γ_L) and power reflected from the right (Γ_R) at the Bragg frequency f_B as a function of the gain/ loss parameter n_I in structure of 150 number of periods, $n_R = 1.55$ and $\Delta n_R = 0.01$ for 2 different amplitudes of the input of CW signal (a) $E_m = 0.002E_{sat}$ and (b) $E_m = 0.2E_{sat}$

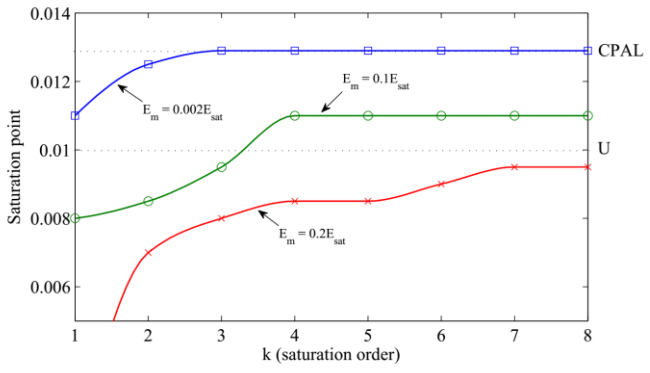

Fig. 4 (Color online) Saturation point as a function of saturation order k for 3 different CW input amplitude.

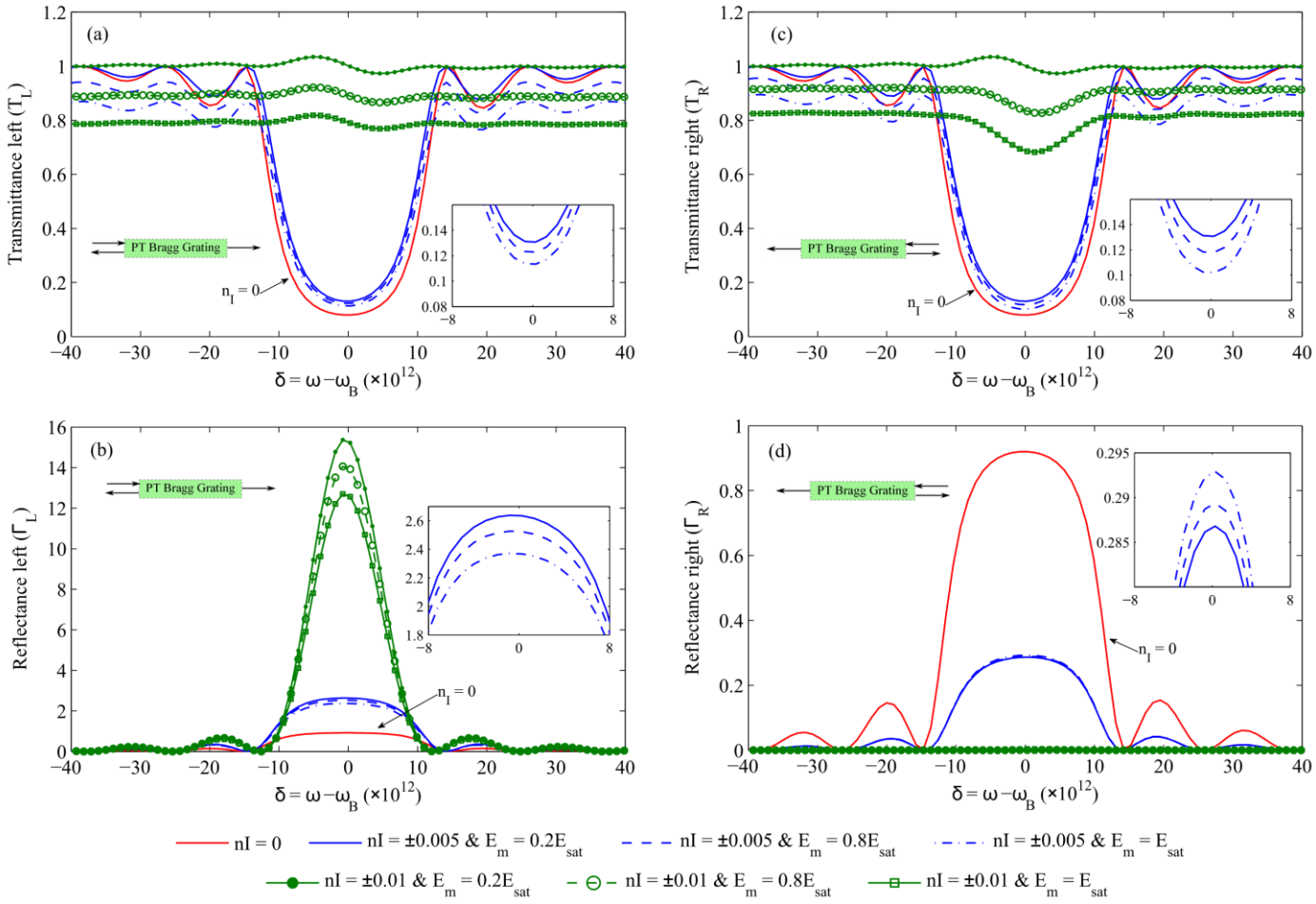

Fig. 5. (Color online) Plot of the spectra of the (a) power transmitted for left (T_L), (b) power reflected for left (Γ_L), (c) power transmitted for right (T_R) and (d) power reflected from the right (Γ_R) obtained using the TLM method for different values of gain/loss parameter n_I and maximum input signal amplitude E_m in a 150 periods grating with $n_R = 1.55$ and $\Delta n_R = 0.01$.

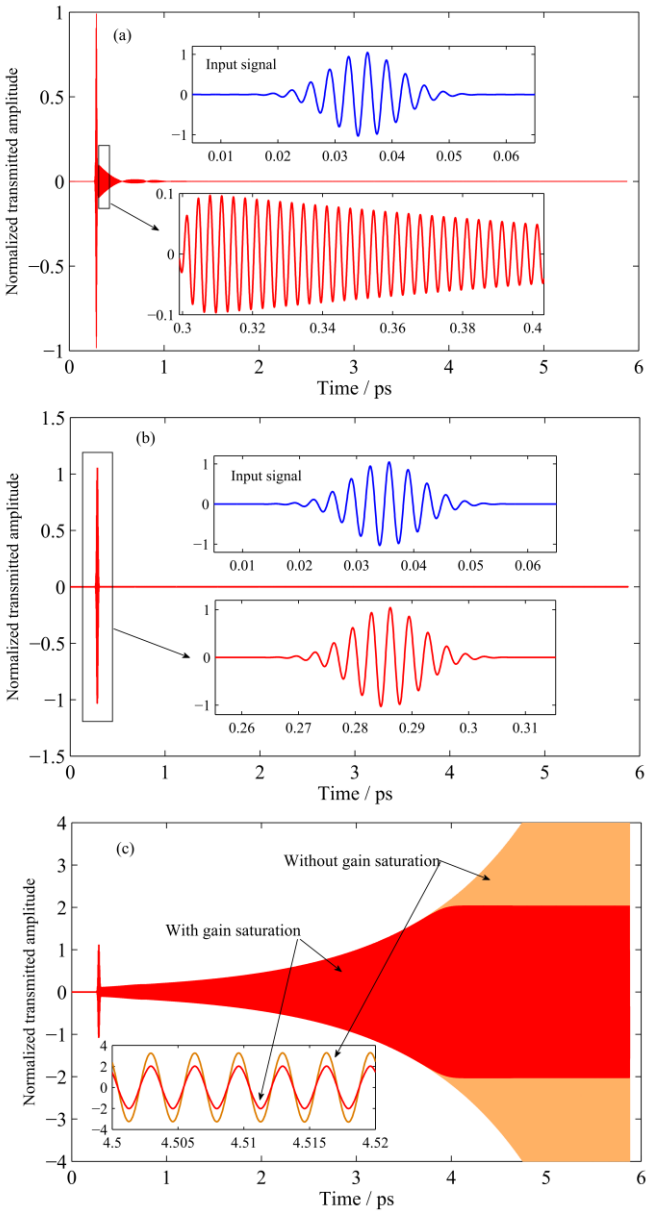

Fig. 6. (Color online) Time domain response of the PT Bragg grating showing transmitted signal for (a) $n_I = 0.0025$, (b) $n_I = 0.01$ and (c) $n_I = 0.013$. The inset of Fig. 5(a) and (b) shows the time domain responses of the input signal to the PT Bragg grating. The inset of fig. 5(c) shows an enlarged view of temporal signal from 4.5 to 4.52 ps of TLM with and without gain saturation model

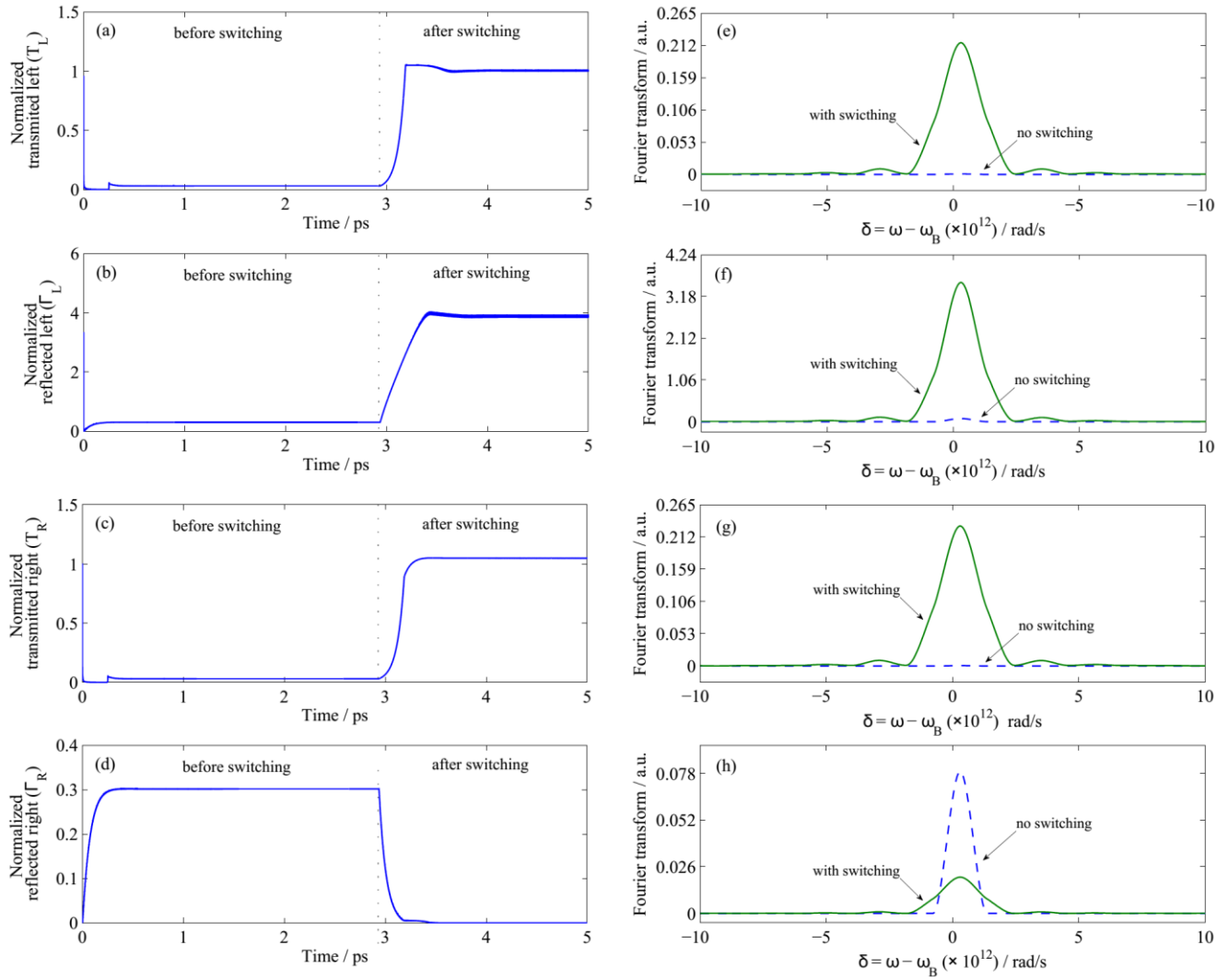

Fig. 7. (Color online) Time (a,b,c,d) and frequency (e,f,g,h) domain response of PT Bragg grating with an instantaneous switching of gain to $n_I = 0.01$ at a time of $t = 3$ps. Excitation is a CW signal at the Bragg frequency f_B. Normalized transmitted T_L (a), and reflected Γ_L (b), signal amplitude envelope for the incidence from the left; Transmitted T_R (c), and reflected Γ_R (d), signal amplitude envelope for the incidence from the right; Frequency response of: (e) T_L, (f) Γ_L, (g) T_R and (h) Γ_R signals with (solid) and without (dashed line) switching. All the frequency domain values are normalized to the frequency domain value of incident signal.

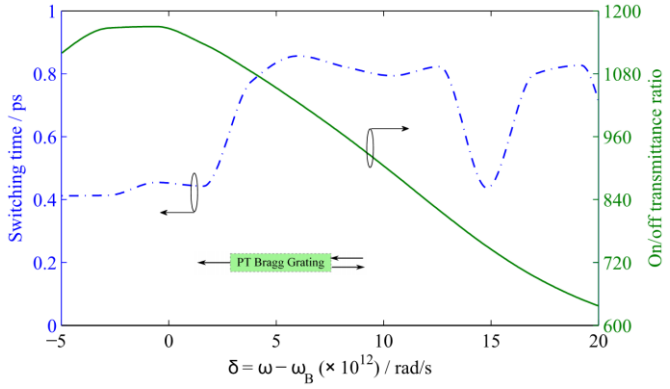

Fig. 8 (Color online) Switching time and on/off transmittance ratio as a function of frequency detuning from the Bragg frequency.

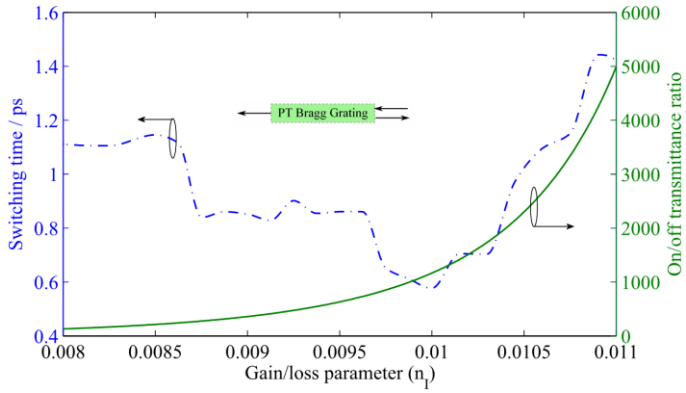

Fig. 9 (Color online) Switching time and on/off transmittance ratio as a function of gain/loss parameter n_l.